On Load-Aware Cell Association Schemes for Group User Mobility in mmWave Networks

Fedor Zhukov*, Olga Galinina†, Eduard Sopin‡, Sergey Andreev†, Konstantin Samouylov‡
*PJSC MegaFon, Moscow, Russia
zhukov.fedor@icloud.com
†Tampere University, Tampere, Finland
{olga.galinina, sergey.andreev}@tuni.fi
‡Peoples' Friendship University of Russia (RUDN), Moscow, Russia
{esopin, ksam}@sci.pfu.edu.ru

***Abstract*—While faster signal attenuation in millimeter wave (mmWave) networks is compensated by high antenna directivity, the effects of dynamic blockages can be mitigated by using connections to multiple access points (APs), and the choice of a proper cell association algorithm plays an essential role in optimizing the overall system performance. Despite numerous research efforts aimed at finding optimal cell associations, effects of user mobility have not been explicitly addressed. Particularly, mobility patterns are imperative in the case of mmWave directional access, as they impact the overall system performance and, thus, might affect the choice of optimal solutions.**

In this paper, we address correlated mobility typical for collective extended reality (XR) applications, using the example of reference point group mobility models (RPGM), where users migrate in groups or clusters. Assuming 3D beamforming and protocol settings of mmWave IEEE 802.11ad/ay that operates at 60 GHz, we compare the performance of two cell association schemes: baseline RSSI-based and load-aware algorithms, and provide important insights on optimization of load-aware scheme parameters, the choice of which is a dynamic function of antenna directivity and network density.

***Index Terms*—Millimeter wave, 60 GHz, 802.11ad/ay, cell association, group mobility, RSSI-based algorithm, load-aware algorithm**

I. Introduction

The emerging popularity of extended reality (XR) applications developed for high-end wireless eyewear imposes stringent connectivity requirements that stem from the nature of human visual perception and include high throughput, extremely low latency, and high link reliability. The expected mass adoption of immersive XR services for wearables will cause significant network densification, which cannot be handled by legacy wireless protocols operating in licensed or unlicensed spectrum. This, in turn, requires the use of more advanced radio technologies [1].

To meet the agressive connectivity requirements, vendors and standardization bodies shift their attention to a less crowded millimeter wave (mmWave) spectrum that offers wideband connectivity and promises to support multi-gigabit data rates. The core features of mmWave propagation encompass much stronger signal attenuation in comparison to that in lower frequencies, high penetration losses, and weak ability to diffract around obstacles that leads to frequent and unpredictable blockage [2]. For example, an average human body attenuates the mmWave signal by up to 35 dB [3]–[5], wall materials contribute even higher losses, up to 80 dB [6].

While faster signal attenuation is partially compensated by highly directional transmission, the effects of dynamic blockage can only be mitigated by taking advantage of maintaining connections to multiple access points (APs) and selecting those, which are able to provide a line-of-sight (LoS) link [5]. In that regard, cell association algorithms play an essential role in optimizing the mmWave system performance, and the research community actively studies their implementation in mmWave networks. In general, cell association mechanisms are conventionally based on solving an optimization problem, where the objective function represents either the network throughput with guaranteed fairness [7] or without it [8], [9], or AP utilization [10].

Despite the existing efforts aimed at finding optimal associations, effects of user mobility have not been explicitly addressed in past literature. Particularly, mobility patterns are important in the case of mmWave-based directional access as they considerably impact the overall system performance and, thus, may affect the choice of optimal solutions. For collective XR services, of special interest become the models with correlated travel trajectories, where users migrate in groups or clusters.

In this paper, we address a mobile scenario with correlated XR user mobility and compare the performance of two cell association schemes: baseline received signal strength (RSSI) based algorithm [11] and load-aware algorithm under realistic mmWave protocol settings. In particular, we assume that wireless connectivity is controlled by a protocol with the structure and timings similar to the IEEE 802.11ad/ay operating in the unlicensed 60 GHz band, and the network users move according to the reference point group mobility (RPGM) model [12]. Consequently, our study incorporates three elements of mmWave network modeling essential for selecting an appropriate cell association approach: (i) specifics of the channel and antenna directionality, (ii) realistic protocol structure and 3D beamforming, and (iii) a user mobility patterns typical for the implied XR scenario.

The remainder of this paper is organized as follows. In Section II, we briefly summarize the main principles of 802.11ad/ay operation, which are essential for our scenario. Section III outlines the modeling parameters and our main assumptions, while Section IV introduces the considered RSSI-based and load-aware algorithms. Finally, Section V illustrates selected numerical results, while Section VI concludes the paper.

II. IEEE 802.11AD/AY STRUCTURE

In the unlicensed spectrum, which is expected to accommodate the traffic of most non-cellular mmWave-based XR headsets, the IEEE 802.11 family offers two wireless standards for operating in the 60 GHz band: commercially available 802.11ad developed in 2012 [13], which promises theoretical data rates of up to 7 Gbps [14], [15], and its latest improvement – 802.11ay [16] expected to be approved in 2020 and deliver the data rates of up to 275 Gbps. In this section, we highlight the core protocol details specified by IEEE 802.11ad/ay that we incorporate in our modeling.

1) Beacon interval structure: Following the principles of the legacy Wi-Fi standards, the medium access in 802.11ad/ay is organized based on periodic beacon intervals (BIs), and the schedule is controlled by an AP. Every BI is divided into (i) a beacon header interval (BHI) controlling initial access and synchronization, and (ii) a data transmission interval (DTI), where the connected devices directly exchange their data packets (see Fig. 1). The BHI, in turn, contains a beacon transmission interval (BTI), where the AP broadcasts directional beacons to non-AP devices, an optional association beamforming training (A-BFT) interval dedicated to beamforming of antennas of non-AP devices, and an announcement transmission interval (ATI) designed for request-response management information exchange. The DTI, which follows the BHI, consists of contention-based access periods (CBAPs) based on enhanced distributed coordination function (EDCF) and scheduled service periods (SPs), where paired devices communicate without contention. A detailed description of channel access principles can be found in [14]–[16].

2) Beamforming: Beamforming in 802.11ad/ay, during which the communicating devices identify their best antenna configuration, is split into two phases: sector-level sweep (SLS) implemented during BTI and A-BFT intervals, and beam refinement phase (BRP) in DTI. During the SLS, the initiating beamforming station (termed initiator) and the responding device (termed responder) exchange a series of directional sector sweep (SSW) frames using omnidirectional reception. Based on the strongest received signal, the devices identify the best transmit sectors, i.e., the initial transmit antenna configuration that can be refined later on. Hence, after the A-BFT interval, coarse beamforming is completed, and in the ATI, the devices exchange management information – including the upcoming schedule – by using directional transmission.

To increase the directivity transmit/receive gain, the information regarding the best antenna configuration identified in the SLS can be further improved during the BRP phase, which precedes the actual data transmission in DTI. The BRP phase may include both transmit beam refinement within the known direction and receive beam training for the paired devices.

III. SYSTEM MODEL AND ASSUMPTIONS

In this section, we outline our core system-level assumptions and introduce the main modeling parameters.

1) System geometry and mobility: We consider a square area of interest with the side of D. The area is populated with N_{UE} mobile users served by N_{AP} mmWave APs that are evenly distributed to provide sufficient coverage. The user devices are elevated at h_{UE} from the ground, while the height of the APs is set to h_{AP}.

The UEs are traveling across the area of interest according to the RPGM model, as illustrated in Fig. 2. In particular, the users form a cluster, the logical center of which defines the mobility pattern of the entire group. The cluster center moves with the constant speed v between random, uniformly distributed locations, where it pauses for a time interval drawn from the exponential distribution with the average of $\bar{\tau}$. During the pause time, the users remain within a circle of radius r around the cluster center, and their positions are random, uniformly distributed in the circle, and independent of the location at the previous step. Between the pause positions, the users travel with constant speed. An example RPGM trajectory is illustrated in Fig. 2.

2) Antenna properties: Each user in our scenario is equipped with a mmWave antenna that can be steered in both vertical and horizontal planes. In particular, we assume that during the initial beamforming phase in the SLS, all antennas can sweep through $K_{\text{V,S}}$ vertical and $K_{\text{H,S}}$ horizontal directions, i.e., yielding $K_{\text{S}} = K_{\text{V,S}} \cdot K_{\text{H,S}}$ SSW sectors. For additional beam refinement, an SSW can be further subdivided into $K_{\text{V,R}}$ and $K_{\text{H,R}}$ narrow directions, so that the total number of sectors can be increased to $K_{\text{R}} = K_{\text{V,S}} K_{\text{H,S}} K_{\text{V,R}} K_{\text{H,R}}$.

One sector is covered by a beam with the azimuth and elevation half power beamwidth (HPBW) of ϕ_{HPBW} and θ_{HPBW}, correspondingly. We select the HPBW such that the power within one beam (immediately after the beam training) may decrease by not more than -3 dB, which is equivalent to

$$\phi_{\text{HPBW}} = \frac{\Omega_V}{4\pi K_{\text{V}}}, \quad \theta_{\text{HPBW}} = \frac{\Omega_H}{4\pi K_{\text{H}}}, \tag{1}$$

where $K_{\text{V}}/K_{\text{H}}$ denote the total number of vertical/horizontal beam directions covering solid angles Ω_V/Ω_H, correspondingly. For example, in our scenario, we assume that AP antennas are downtilted, and all beams cover only the lower hemisphere, and hence, $\Omega_V = 2\pi$ for the both receive and transmit AP antenna modes. The situation is symmetrical for the UEs, where antenna beams are assumed to cover the upper hemisphere, i.e., $\Omega_V = 2\pi$. In the horizontal plane, UE and AP transmit/receive beams can be steered through the solid angle $\Omega_H = 4\pi$.

The resulting HPBW defines the directional antenna gains for both reception and transmission. To address the effects of azimuth and elevation beam misalignment, we utilize the

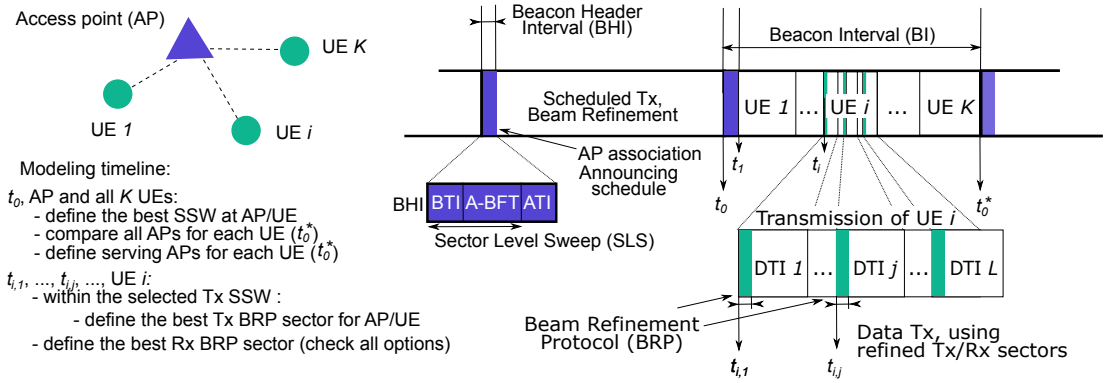

Fig. 1: Illustration of beacon interval structure and main beamforming phases.

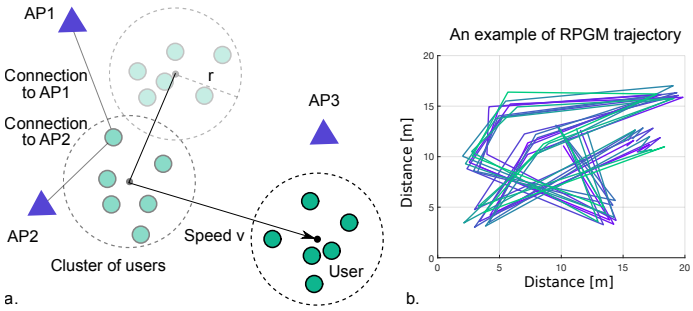

Fig. 2: Illustration of group mobility in our scenario.

MiWeba model [17] and assume that the antenna gain in decibels can be expressed via ϕ and θ as

$$G_{\text{dB}}(\phi,\theta) = 10\log_{10}\left[\frac{16\pi}{6.76\phi_{\text{HPBW}}\theta_{\text{HPBW}}}\right] - 12\left[\frac{\phi}{\phi_{\text{HPBW}}}\right]^2 - 12\left[\frac{\theta}{\theta_{\text{HPBW}}}\right]^2, \quad (2)$$

where ϕ and θ are the azimuth and elevation angles between the antenna boresight direction and the real AP-UE direction.

3) Received power and link throughput: For the known azimuth and elevation beam misalignment at both transmitting and receiving antennas ($\phi_{\text{TX/RX}}$ and $\theta_{\text{TX/RX}}$), the received power may be estimated as

$$P_{\text{RX}} = \eta P_{\text{TX}} G_{\text{TX}}(\phi_{\text{TX}},\theta_{\text{TX}}) G_{\text{RX}}(\phi_{\text{RX}},\theta_{\text{RX}}) L(d, \text{I}_{\text{LOS}}), \quad (3)$$

where η is the antenna efficiency, P_{TX} is the transmit power, G is the transmit/receive antenna gain, and $L(d, \text{I}_{\text{LOS}})$ is the distance-dependent path loss. The path loss at the distance d is calculated according to the Friis propagation equation for the carrier frequency f and reduced by ΔL_{NLOS} in the case of $\text{I}_{\text{LOS}} = 0$. Further, I_{LOS} is the indicator function, which represents the absence of blockers and, hence, the presence of LoS connection. It is generated by a stochastic ON-OFF process, where time intervals are distributed exponentially with the average $\bar{\tau}_{\text{NLOS}}$ and $\bar{\tau}_{\text{LOS}}$, respectively.

We estimate the link data rate using the Shannon's formula:

$$R_{\text{inst}} = B\log_2(1 + \min(\text{SNR}, \text{SNR}_{\max})), \quad (4)$$

where B is the channel bandwidth, SNR is the signal-to-noise ratio, and $\text{SNR}_{\max}$ corresponds to the best modulation-coding scheme (MCS).

The actual data rate at the UE can be defined based on the allocated time resource that depends on the number of UEs and the overhead, as

$$R_{\text{act}} = s \cdot C = s \cdot B\log_2\left(1 + \min(\tfrac{P_{\text{RX}}}{N_0}, \text{SNR}_{\max})\right), \quad (5)$$

where s is the share of radio resources dedicated to the data transmission of one user and N_0 is the noise power.

Notation	Definition	Value
D	Size of area of interest	20 m
N_{AP}	Number of APs	4
h_{AP}	AP height	10 m
N_{UE}	Number of UEs	20
h_{UE}	UE height	1.5 m
v	Cluster speed	3 kmph
$\bar{\tau}$	Average pause time	5 s
r	Cluster radius	3 m
f_c	Carrier frequency	60 GHz
P_{TX}	Transmit power	0 dBm
B	Bandwidth	1 GHz
T_{BI}	Beacon interval	1000 ms
N_0	Noise level	-90 dBm
$\text{SNR}_{\max}$	SNR corresponding to best MCS	15 dB
	AP azimuth range	[0°,360°]
	AP elevation range	[180°,360°]
	UE azimuth range	[0°,360°]
	UE elevation range	[0°,180°]
K_{H}	Number of SSW in azimuth	4
K_{V}	Number of SSW in elevation	2
M_{BRP}	Number of BRP sectors per one SSW	3
	BRP sector width	[30°, 18°, 9°]
$T_{\text{BRP}}(n_s)$	BRP overhead for n_s sectors	0.016+$n_s \cdot$ 0.0007 ms
T_{BHI}	BHI overhead	0.1 ms
T_{conn}	AP connection overhead	$T_{\text{BI}}/2$

TABLE I: System parameters

4) Protocol settings: In our setup, we assume a scheduler, which equally divides the available DTI time among all users. Hence, the share of one user may be expressed as

$$s = \frac{\left(\frac{T_{\text{BI}} - T_{\text{BHI}}}{N}\right) - T_{\text{BRP}} M_{\text{BRP}}}{T_{\text{BI}}} = \frac{T_{\text{BI}} - T_{\text{BHI}} - T_{\text{BRP}} N M_{\text{BRP}}}{N T_{\text{BI}}}, \quad (6)$$

where T_{BI} is the variable BI length, T_{BHI} is the fixed duration of the BHI, T_{BRP} is the overhead that is produced by the BRP procedure, and M_{BRP} is the number of BRP trainings during a service period of one user. We assume that all the devices have the same antenna settings, and, therefore, $T_{\text{BRP}}(n_s)$, which depends on the total number n_s of BRP sectors, is fixed across

the considered network. The overhead parameters are given in Table I, where AP connection overhead T_{conn} denotes the time required to switch a connection to another AP.

IV. Considered algorithms

In this section, we sketch two cell-association algorithms, particularly, RSSI-based and load-aware schemes, which we assess further in Section V.

A. RSSI-based algorithm

The basic principle of the RSSI-based algorithm is in selecting a serving AP, whose RSSI during the SLS phase is stronger at the considered UE (in our scenario, all UEs continuously measure the signal from all APs). To add more flexibility in decision making and avoid oscillations, we introduce probability p of changing the serving AP for the one with the better RSSI; p is fixed across the network. Consequently, if $p = 1$, UEs will always be associated with the same AP that was selected at the initial stage of the system operation. On the contrary, in the case of $p = 0$, UEs immediately switch to better APs.

We note that in reality, BIs of different APs begin at non-synchronized time moments. However, since UEs may sense the channel and collect the information on all other APs over one BI, we, for the sake of simplicity, may consider a system where BIs of all APs are fully synchronized. The difference between these two systems is that for non-synchronized BIs (i) the information on the previous RSSI values of other APs is more recent than that of the serving station and (ii) in the case of a decision to change the serving AP, the UE is forced to wait for the respective BHI, which creates an additional delay as compared to the synthetic synchronized system. We disregard the effects of the first fact, but to accommodate the second, we introduce a penalty (the AP overhead) that is represented by an extra delay when the UE cannot transmit. We assume that in the non-synchronized system, the begin times of BIs are randomly distributed, and therefore, the corresponding expected delay, i.e., the penalty in the synchronized system, equals $T_{\text{BI}}/2$.

As such, in the synchronized system, the UEs collect all the information regarding the RSSI values from all APs by the beginning of the new BHI and make their decisions on selecting the serving AP. After selecting the target AP, in the corresponding new BHI, the UE requests DTI resources and is further served after beam training in the BRP phase. The considered scheme is outlined in Algorithm 1.

B. Load-aware algorithm

The load-aware algorithm allows the UEs to choose their serving AP based on the expected throughput precalculated based on the previous RSSI values and the predicted share of UEs. The effective timeshare at any candidate AP may be approximately estimated by a UE if the APs broadcast the load during their recent BI. By the beginning of each BI, the considered UE is aware of the previous RSSI and load values from all APs; the expected data rate is then calculated by equation (5). Here, we also rely on probability p for adjusting the UE decisions on selecting a new serving AP (see Algorithm 2 for pseudocode of the load-aware scheme). By analogy with the RSSI-based algorithm, in the case of $p = 1$, UEs remain associated with their initial APs, and alternatively, $p = 0$ forces UEs to immediately connect to the APs with the better expected throughput. Following the same logic as above, we further consider a synchronized system with the penalty for switching to the new AP.

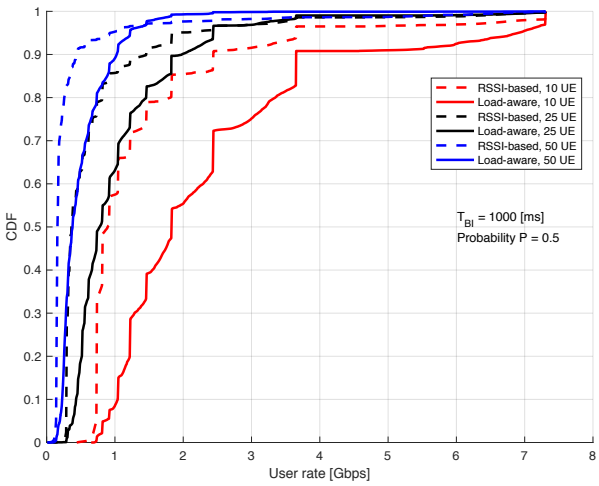

Fig. 3: Data rate CDF of RSSI-based and load-aware algorithms for varying UE population

V. Numerical results

In this section, we provide selected numerical results for the two implemented cell association algorithms described in Section IV. In what follows, we follow the numerology of IEEE 802.11ay assuming one spacial stream and one channel, while setting by default $T_{\text{BI}} = 1000$ ms and $p = 0.5$. The resulting data rate is measured on a micro-scale, i.e., within each BI, so that the resulting simulation incorporates the effects of beam misalignment, which occurs between all the consequent beam training procedures due to the user mobility.

We begin with analyzing the cumulative distribution function (CDF) of the average UE data rate achieved in the case of the RSSI-based and load-aware association algorithms for a varying user population, as shown in Fig. 3. The results demonstrate a clear advantage of the load-aware algorithm over the RSSI-based scheme, independently of the number of users in the area of interest. The gap between the performance of these two association algorithms decreases with the growing UE population, which is explained by a general decrease in the data rate due to smaller UE shares. The relative gain of the load-aware scheme remains the same: e.g., for the 50th percentile (middle quantile), the data rate improvement reaches 100% as compared to the RSSI-based scheme. The stair-like shape of the CDFs in Fig. 3 is the result of introducing MCS limitation that affects the maximum data rate.

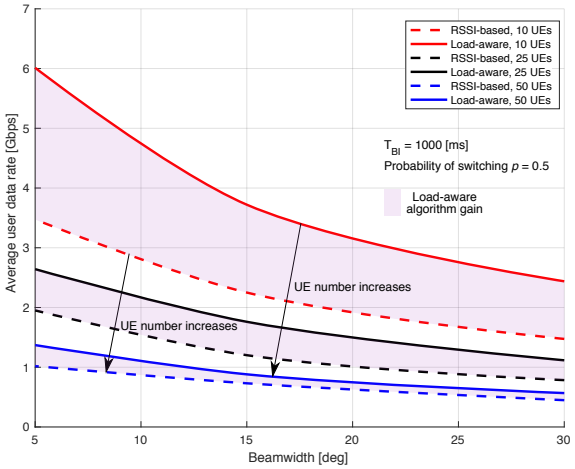

Fig. 4: Average user rate of RSSI-based and load-aware algorithms for varying beamwidth and UE population

Further, we investigate the impact of mmWave antenna directivity on the average user data rate averaged over the time of UE operation and all the UEs in the system. For example, Fig. 4 illustrates the benefits of using highly-directional antennas for both load-aware and RSSI-based association algorithms. In the case of 10 UEs, the beamwidth expansion by only 10 degrees leads to a degradation of the average user data rate by almost 30%, and this trend maintains for other UE populations. With respect to the number of UEs, we may observe the gains of the load-aware scheme similar to those that Fig. 3 reports. Regardless of the number of UEs and the beamwidth, the load-aware algorithm provides a higher average user data rate.

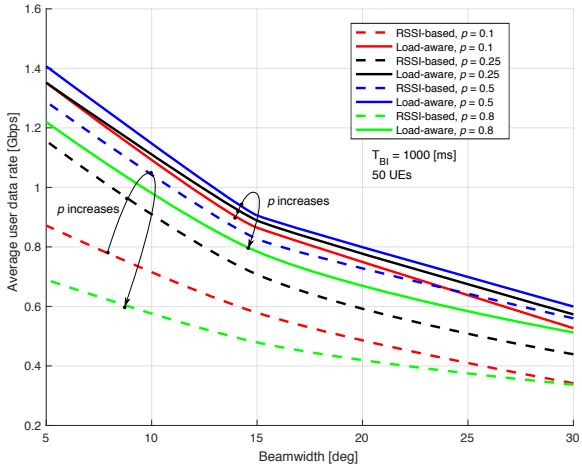

Fig. 5: Average user rate of RSSI-based and load-aware algorithms applying varying beamwidth and probability p

Finally, Fig. 5 illustrates the impact of the choice of p on the average data rate across a range of the potential antenna beamwidths. Here, we may notice that an increased value of p results in improved average data rate; however, starting at a certain point, the performance degrades rapidly. Hence, there exists an optimal value p^*, which depends on a set of parameters, including the mobility speed and pattern, the selected beamwidth, and the protocol settings, such as the length of the BI and the frequency of BRP procedures. Interestingly, the RSSI-based algorithm with probability $p = 0.5$ (blue dashed line) performs better than the load-aware algorithm with probability $p = 0.8$ (green solid line) and, therefore, adequate choice of p is an important matter.

Algorithm 1 RSSI-based algorithm

Input: N_{AP}, N_{UE}, locations of APs, locations and mobility patterns of UEs, switching probability p, number of BIs N_{BI}
Output: UE data rate set

Initialize AP set = $[1, ..., N_{\text{AP}}]$, UE set = $[1, ..., N_{\text{UE}}]$
Initialize serving AP set = $\emptyset$, UE data rate set = $\emptyset$
InitialRSSIAssociation() // RSSI-based only
//Cell-association and service
for all beacon intervals $b_i, i \in [1, N_{\text{BI}}]$ **do**
  UE data rate set $\leftarrow$ ServeUEs (serving AP set)
  for all $u \in [1, ..., N_{\text{UE}}]$ **do**
    for all $a \in [1, ..., N_{\text{AP}}]$ **do**
      Measure received power $P_{\text{RX}}(u, a, b_i)$ at u
    end for
    Candidate AP $a^c(u, b_i) \leftarrow \arg \max_{a \in [1,...,N_{\text{AP}}]} P_{\text{RX}}(u, a, b_i)$
    Generate $s \in \{0, 1\}$ with probability $\{1 - p, p\}$
    if $s = 0$ **then**
      Serving AP changes $a^s(u, b_{i+1}) \leftarrow a^c(u, b_i)$
    else
      Serving AP is the same $a^s(u, b_{i+1}) \leftarrow a^s(u, b_i)$
    end if
    Update serving AP set
  end for
end for

VI. Conclusions

In this paper, we provide a comparison of two mmWave cell-association algorithms: the baseline RSSI-based scheme and a more advanced load-aware approach that takes advantage of the information on the current AP loading that may be broadcasted to all the network users. Our model incorporates three important parts: (i) specifics of mmWave propagation, antenna directivity, and 3D beamforming, (ii) mmWave protocol features (by example of IEEE 802.11ad/ay) that include periodic beamforming, scheduling, and more frequent beam refinements, and (iii) dynamic user mobility. We particularly address group mobility, where users may migrate across the area of interest in clusters, as the network performance in this case is largely dependent on the immediate user density.

In general, the load-aware cell association scheme outperforms the conventional RSSI-based algorithm in terms of the UE data rate; however, parametrization of the load-aware scheme requires more complex analysis and optimization. Since the emerging mmWave systems are envisioned to be highly dynamic in terms of user mobility and blockage, the parameters of the load-aware algorithm should also remain dynamic. They may be estimated based on the user history and a window of loading and RSSI values by using predictive analytics.

function ServeUEs (serving AP set)
Input: N_{AP}, N_{UE}, locations of APs, locations and mobility patterns of UEs
Output: UE data rate set

```
for all a ∈ [1, ..., N_AP] do
  Initial SSW
  Serving AP a shares resources between associated UEs
  for all users u from serving AP a set do
    for m = 1, ..., M_BRP do
      BRP procedure
      u is served with directional beams defined by BRP
    end for
  end for
end for
```

function InitialAssociation()
Input: N_{AP}, N_{UE}, locations of APs, initial locations of UEs
Output: Serving AP set (full info about associations)

```
for all u ∈ [1, ..., N_UE] do
  for all a ∈ [1, ..., N_AP] do
    Measure received power P_RX,0(u, a) at u
  end for
  Serving AP a^s(u, b_1) ← arg max_{a∈[1,...,N_AP]} P_RX,0(u, a)
  Update serving AP set
end for
```

Algorithm 2 Load-aware algorithm

Input: N_{AP}, N_{UE}, locations of APs, locations and mobility patterns of UEs, switching probability p, number of BIs N_{BI}
Output: UE data rate set

```
Initialize AP set = [1, ..., N_AP], UE set = [1, ..., N_UE]
Initialize serving AP set = ∅, UE data rate set = ∅
InitialRSSIAssociation() // RSSI-based only
for all a ∈ [1, ..., N_AP] do
  Estimate the number of UEs connected to AP and define
  share s(a, u, b_1) for each u that belongs to a
end for

//Cell-association and service
for all beacon intervals b_i, i ∈ [1, N_BI] do
  UE data rate set ← ServeUEs(serving AP set)
  for all u ∈ [1, ..., N_UE] do
    for all a ∈ [1, ..., N_AP] do
      Measure received power P_RX(u, a, b_i) at u
      Define immediate throughput T_i(u, a, b_i)
      Expected T_exp(u, a, b_i) ← s(a, u, b_1)T_i(u, a, b_i)
    end for
    Candidate AP a^c(u, b_i) ← arg max_{a∈[1,...,N_AP]} T_i(u, a, b_i)
    Generate s ∈ {0, 1} with probability {1 − p, p}
    if s = 0 then
      Serving AP changes a^s(u, b_{i+1}) ← a^c(u, b_i)
    else
      Serving AP is the same a^s(u, b_{i+1}) ← a^s(u, b_i)
    end if
    Update serving AP set
  end for
  for all a ∈ [1, ..., N_AP] do
    Estimate s(a, u, b_{i+1}) for each u that belongs to a
  end for
end for
```

REFERENCES

[1] L. Han, S. Appleby, and K. Smith, "Problem statement: Transport support for augmented and virtual reality applications," 2017. [Online; accessed August 2019].

[2] S. Rangan, T. S. Rappaport, and E. Erkip, "Millimeter wave cellular wireless networks: Potentials and challenges," *arXiv preprint arXiv:1401.2560*, 2014.

[3] S. Rajagopal, S. Abu-Surra, and M. Malmirchegini, "Channel feasibility for outdoor non-line-of-sight mmwave mobile communication," in *2012 IEEE Vehicular Technology Conference (VTC Fall)*, pp. 1–6, IEEE, 2012.

[4] J. S. Lu, D. Steinbach, P. Cabrol, and P. Pietraski, "Modeling human blockers in millimeter wave radio links," *ZTE Communications*, vol. 10, no. 4, pp. 23–28, 2012.

[5] G. George, K. Venugopal, A. Lozano, and R. W. Heath, "Enclosed mmwave wearable networks: Feasibility and performance," *IEEE TWC*, vol. 16, no. 4, pp. 2300–2313, 2017.

[6] A. V. Alejos, M. G. Sanchez, and I. Cuinas, "Measurement and analysis of propagation mechanisms at 40 GHz: Viability of site shielding forced by obstacles," *IEEE TVT*, vol. 57, no. 6, pp. 3369–3380, 2008.

[7] Y. Xu, H. Shokri-Ghadikolaei, and C. Fischione, "Auction based dynamic distributed association in millimeter wave networks," in *2016 IEEE Globecom Workshops (GC Wkshps)*, pp. 1–6, IEEE, 2016.

[8] H. Shokri-Ghadikolaei, Y. Xu, L. Gkatzikis, and C. Fischione, "User association and the alignment-throughput tradeoff in millimeter wave networks," in *2015 IEEE 1st International Forum on Research and Technologies for Society and Industry Leveraging a better tomorrow (RTSI)*, pp. 100–105, IEEE, 2015.

[9] Y. Xu, H. Shokri-Ghadikolaei, and C. Fischione, "Distributed association and relaying with fairness in millimeter wave networks," *IEEE TWC*, vol. 15, no. 12, pp. 7955–7970, 2016.

[10] G. Athanasiou, P. C. Weeraddana, C. Fischione, and L. Tassiulas, "Optimizing client association for load balancing and fairness in millimeter-wave wireless networks," *IEEE/ACM Transactions on Networking*, vol. 23, no. 3, pp. 836–850, 2014.

[11] Y. Bejerano, S.-J. Han, and L. E. Li, "Fairness and load balancing in wireless LANs using association control," in *Proceedings of the 10th annual international conference on Mobile computing and networking*, pp. 315–329, ACM, 2004.

[12] X. Hong, M. Gerla, G. Pei, and C.-C. Chiang, "A group mobility model for ad hoc wireless networks," in *Proceedings of the 2nd ACM international workshop on Modeling, analysis and simulation of wireless and mobile systems*, vol. 53, 1999.

[13] "IEEE Standard for Information Technology–Telecommunications and information exchange between systems–Local and metropolitan area networks–Specific requirements-Part 11: Wireless LAN Medium Access Control (MAC) and Physical Layer (PHY) Specifications Amendment 3: Enhancements for Very High Throughput in the 60 GHz Band," 2012.

[14] T. Nitsche, C. Cordeiro, A. B Flores, E. W. Knightly, E. Perahia, and J. Widmer, "IEEE 802.11ad: directional 60 GHz communication for multi-Gigabit-per-second Wi-Fi," *IEEE Communications Magazine*, vol. 52, no. 12, pp. 132–141, 2014.

[15] E. Perahia, C. Cordeiro, M. Park, and L. L. Yang, "IEEE 802.11ad: Defining the next generation multi-Gbps Wi-Fi," in *2010 7th IEEE CCNC*, pp. 1–5, IEEE, 2010.

[16] Y. Ghasempour, C. R. da Silva, C. Cordeiro, and E. W. Knightly, "IEEE 802.11ay: Next-generation 60 GHz communication for 100 Gb/s Wi-Fi," *IEEE Communications Magazine*, vol. 55, no. 12, pp. 186–192, 2017.

[17] R. J. Weiler, M. Peter, W. Keusgen, A. Maltsev, I. Karls, A. Pudeyev, I. Bolotin, I. Siaud, and A.-M. Ulmer-Moll, "Quasi-deterministic millimeter-wave channel models in MiWEBA," *EURASIP Journal on Wireless Communications and Networking*, vol. 2016, no. 1, p. 84, 2016.